Time and Frequency Resolution of Alternating Electric Signals via Single-Atom Sensor

Y.-Q. Wei,[1,2,‡] Q. Yuan,[1,3,‡] L. Chen,[1,4,*] T.-H. Cui,[1,3] J. Li,[1,3] S.-Q. Dai,[1,3] F. Zhou,[1,4] and M. Feng[1,4,5,†]

[1] *State Key Laboratory of Magnetic Resonance and Atomic and Molecular Physics, Wuhan Institute of Physics and Mathematics, Innovation Academy of Precision Measurement Science and Technology, Chinese Academy of Sciences, Wuhan 430071, China*

[2] *Laboratory of Quantum Science and Engineering, South China University of Technology, Guangzhou 510641, China*

[3] *University of the Chinese Academy of Sciences, Beijing 100049, China*

[4] *Research Center for Quantum Precision Measurement, Guangzhou Institute of Industry Technology, Guangzhou, 511458, China*

[5] *Department of Physics, Zhejiang Normal University, Jinhua 321004, China*

(Received 1 July 2022; revised 27 April 2023; accepted 26 May 2023; published 21 June 2023)

The characterization of externally applied signals is essential in order to improve performance and design appropriate engineering strategies in cold-atom experiments. Here, we present a practical technique to detect the artificially introduced electric signals by an exquisite sensor made of a single $^{40}Ca^{+}$ ion behaving as the phonon laser. The sensor can work as an oscilloscope, detecting spectra of the signals in the time domain, and also as a frequency spectrograph for the signal probe with respect to the frequency. The high precision of such an atomic sensor relies on the unique characteristics of the phonon laser. In particular, the sensor is practical since it works without the prerequisite of sideband cooling and the performance of the sensor can be further improved depending on better trapping conditions and a higher collection efficiency of the spontaneous emission fluorescence.

DOI: 10.1103/PhysRevApplied.19.064062

I. INTRODUCTION

Optical and electric pulses are ubiquitous in all physical operations. In particular, with the rapid development of quantum techniques, the characterization of externally applied signals has become a key challenge in quantum information processing [1–6], which is experimentally relevant to the design of appropriate engineering strategies and improving the performance of the alternating pulses.

In this work, we demonstrate a practical technique, using a single cold trapped ion as the atomic sensor, to detect the artificially introduced electric signals. The laser-cooled ions confined in the electromagnetic potential are a promising candidate for precisely measuring electric field variations, since they are charged themselves and extremely sensitive to the electric field fluctuations [7–9]. In this sense, what we detect is not just relevant to the input pulses for operations but also associated with the unexpected electric field fluctuations in the systems. In ion traps, the electric field fluctuations are typical types of noise, leading to instability of the trapped ions, i.e., the main detrimental factor for confining and manipulating the ions [10]. As a result, our technique might be useful for understanding and thus suppressing the electric field fluctuations.

Our experiment is carried out in a surface-electrode trap (SET) that confines a single trapped ion. The key point of the sensor is that the trapped ion behaves as an injection-locked phonon laser, i.e., an amplitude-amplified harmonic oscillator, which is quite sensitive to the external disturbance, as reported previously [11–16]. In our experiment, the ion is first Doppler cooled and then excited to be the state of the phonon laser, which is locked onto the oscillation frequency by an injection-locking signal. We present two sets of experiments to probe the spectra of the signal in the time and frequency domains, which function like an oscilloscope and a frequency spectrograph, respectively. Our probing technique and results have the following distinct features. The technique enables a credible probing of the electric field variations with high precision, based on the sensitive features of the phonon laser to the ac electric field fluctuation in the SET, which has achieved an ac electric force detection sensitivity in the yoctonewton (1 yN $= 10^{-24}$ N) range [17]. Moreover, our detection works

*liangchen@wipm.ac.cn
†mangfeng@wipm.ac.cn
‡Co-first authors with equal contribution.

without the prerequisite of sideband cooling, reducing the experimental challenge considerably. Furthermore, in principle, our technique favors detection of the external signals with all frequencies and with tiny amplitude variations. This implies that our presented probe might be applicable to the detection of real environmental noise in the trapped-ion system in the future. In all, this technique is not mainly limited by the temperature of the ion but the stability of the characteristic parameters of the trapping system, as elucidated later.

II. EXPERIMENTAL SYSTEM AND SCHEME

Our experiment is carried out using a single trapped $^{40}Ca^{+}$ ion in the SET, which is a 500-μm-scale planar trap as introduced previously [18–20]. Figure 1 presents a schematic diagram of the setup and the method in our experiment. The measured secular frequencies of the SET are, respectively, $\omega_z/2\pi = 183.41 \pm 0.01$ kHz, $\omega_x/2\pi = 532.10 \pm 0.10$ kHz, and $\omega_y/2\pi = 838.50 \pm 0.10$ kHz. The single $^{40}Ca^{+}$ ion, which stays 800 μm above the surface of the SET, behaves as a phonon laser in the potential. The phonon laser is produced by the oscillation amplification of the ion stimulated by two 397-nm laser beams, one of which is red detuned with detuning $\Delta_r/2\pi = -80$ MHz and the other of which is blue detuned with $\Delta_b/2\pi = 40$ MHz. Both of the laser beams are elaborately tuned to have the appropriate intensity ratio $r = I_b/I_r = 0.5$ in order to keep the oscillation amplification stable [11], which yields a phonon laser with an oscillation amplitude of 22.14 μm. Furthermore, the phonon laser applies solely to the z-axis motional degree of freedom of the ion due to the large frequency differences in different directions.

Throughout the work, we may lock the z-axis oscillation frequency of the phonon laser by applying an appropriate injection-locking signal to the AE electrode, which has no influence on other two directions. We input the artificially generated signals and the injection-locking signal into the system from the AE electrode. Since both of them are ac signals, we need to couple them to the electrodes through the capacitors, i.e., C_3 and C_4. Additionally, we have C_1, C_2 and L_1 forming a π-type filter, i.e., a low-pass filter to filter the radio-frequency (rf) signal, where C_2 works for damping both the injection locking and the additionally applied signals. Since the damping rate is 16 dB, the injection-locking signal or the additionally applied signal felt by the sensor is just 1/40 of the output from the AWG.

Experimentally, the AWG employed is the Keysight 33622A wave-form generator, which generates a signal with frequency ω_n and strength d_n. The signal to be detected is attached to a carrier signal as the amplitude modulation, in the form of $V_n(t) = d_n\delta(\omega_n) \times A_c \sin\omega_c t$, where A_c and ω_c are the amplitude and frequency of the carrier signal, respectively. Four sets of signals are generated in our experiment, including the square-wave signal, the sinusoidal-wave signal, the Gaussian-wave signal, and the white-noise signal, as plotted in Fig. 1(a). These signals represent two kinds of external disturbance, i.e., a periodic signal with frequency ω_n and white noise with the bandwidth ω_n.

For a trapped ion with mass m and oscillation frequency ω_z under the frictional damping γ [11], the dynamics are governed by

$$\ddot{z}(t) + \gamma\dot{z}(t) + \omega_z^2 z(t) = [F(t) + N(t) + S(t)]/m, \quad (1)$$

where $F(t)$ is the injection-locking force that originates from the injection-locking signal $V_i(t) = A_i \sin\omega_i t$ applied on the ion, in which A_i and ω_i are the amplitude and frequency of the injection-locking signal, respectively. The trap frequency ω_z is also the frequency of the phonon laser. Once the injection locking is working, the trapped ion is locked onto the signal, with ω_i approaching ω_z, i.e., $\omega_i \approx \omega_z$, reaching a very narrow bandwidth [22]. $N(t)$ represents the random force due to the thermal noise, which is the origin of the background noise in the system [17]. $S(t)$ is the alternating signal originating from $V_n(t)$ that is introduced artificially for our test.

The straightforward solution of Eq. (1) reads $z(t) = z_0 \sin(\omega_i t + \varphi)$, where z_0 and φ represent the oscillation amplitude and phase of the phonon laser, respectively. Both z_0 and φ vary sensitively with the fluctuation of the electric field [17], where φ, which is directly subject to the injection-locking frequency ω_i, is more sensitive than z_0. We acquire z_0 and φ by the optical method of fitting the fluorescence curve directly obtained from the photomultiplier tube (PMT) [17] (see a brief introduction in Appendix A).

Before detecting the alternating signals, we have to clarify the imprecision of the sensor itself. To this end, we define the responding range Λ of the sensor and experimentally we measure $\Lambda = 0.1$ Hz, which is relevant to our measurement time of 10 s (see Appendix B). As presented in Fig. 1(b), if the frequency ω_n of the signal to be measured is less than 0.1 Hz, we attach the signal to the carrier signal as $V_n(t) = d_n\delta(\omega_n) \times A_c \sin\omega_c t$, as mentioned above. In our case, we simply set the carrier signal to have the same frequency and amplitude as the injection-locking signal, i.e., $A_c = A_i$ and $\omega_c = \omega_i$. In contrast, if ω_n is larger than 0.1 Hz, we still attach the signal to the carrier signal as the amplitude modulation. But in this case we shift the frequency of the carrier signal by Δ_n, i.e., $A_c = A_i$ and $\omega_c = \omega_i + \Delta_n$. The sensor can probe the signal if $|\omega_n - \Delta_n| < \Lambda$ is satisfied [23].

III. EXPERIMENTAL MEASUREMENTS

Since we consider the additionally applied signals to be disturbance to the system, in this section we first define the deviations of our measurements due to the disturbance and

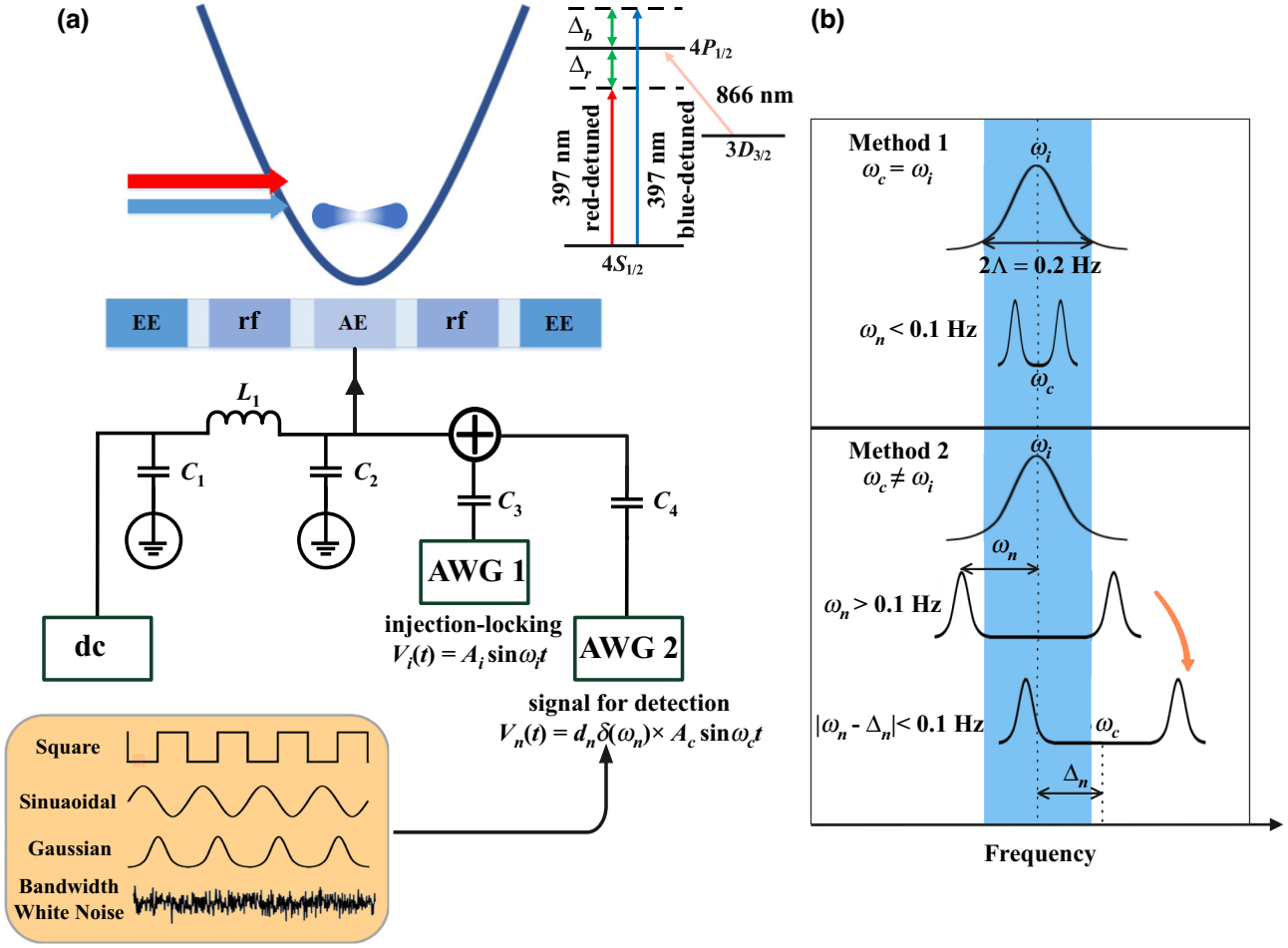

FIG. 1. A schematic for the detection of additionally applied electric signals by the single-ion phonon-laser sensor. (a) The parabola represents a harmonic potential provided by the surface-electrode trap (SET), where the confined Doppler-cooled ion is stimulated to be a phonon laser by a blue-detuned laser (blue arrow) and a red-detuned laser (red arrow). The side view of the SET is plotted, with EE, rf, and AE indicating, respectively, the endcap electrode, the rf electrode, and the axial electrode. Four types of artificially generated electric signals with a wave form of $\delta(\omega_n)$ are input, respectively, into the system from the AE, the electrode to which the injection-locking signal $V_i(t)$ applies. Either the additionally applied or the injection-locking signal is generated by an arbitrary waveform generator (AWG). The additionally applied signal is represented by $V_n(t)$ and is generated by attaching $d_n\delta(\omega_n)$ to the carrier signal $A_c \sin\omega_c t$ as the amplitude modulation. In practice, we set $A_c = A_i$ and ω_c is set depending on ω_n with respect to the responding range Λ of the sensor. The inset on the right-hand side of the parabola is the level scheme of $^{40}Ca^+$ for our purposes, where the 397-nm laser drives the transition between the ground state $4S_{1/2}$ and the excited state $4P_{1/2}$, playing the main role of cooling, and the 866-nm laser couples the $4P_{1/2}$ state to the metastable state $3D_{3/2}$ for repumping of the 6% leakage of spontaneous emission back to $4P_{1/2}$. The detunings Δ_r and Δ_b are defined as the frequency differences of the lasers from the two-level resonance. Since the decay from $P_{1/2}$ to $S_{1/2}$ is much larger than that from $P_{1/2}$ to $D_{3/2}$, the three-level system could be reasonably considered as an effective two-level system [21]. (b) A schematic for two methods of sensing the additionally applied signals in our experiment, where a signal with a sinusoidal wave form is exemplified. The region marked in blue represents the responding range of the single-ion phonon-laser sensor and the dotted line marks the location of the injection-locking frequency. Method 1 works for the case of $\omega_n < \Lambda$, for which the carrier frequency takes the same value as the injection-locking frequency. For Method 2, since $\omega_n > \Lambda$, we have to shift the frequency of the carrier signal by Δ_n.

then present our measurement results for the different types of signals.

A. Definitions of the deviations and error bars

We assume the alternating signals applied to the electrodes to be the dominant factor causing deviation of the detected results. As such, we define the mean deviation $Y = \sum_{i=1}^{N} |dX(i)|/N$, where $dX(i) = X(i) - \bar{X}$ represents the ith measured deviation of the oscillation amplitude z_0 or oscillation phase φ for N measurements. The statistical standard deviation of Y is $dY = \sqrt{\sum_{i=1}^{N} (|dX(i)| - Y)^2/N}$. Based on the above definitions, the relative signal intensity

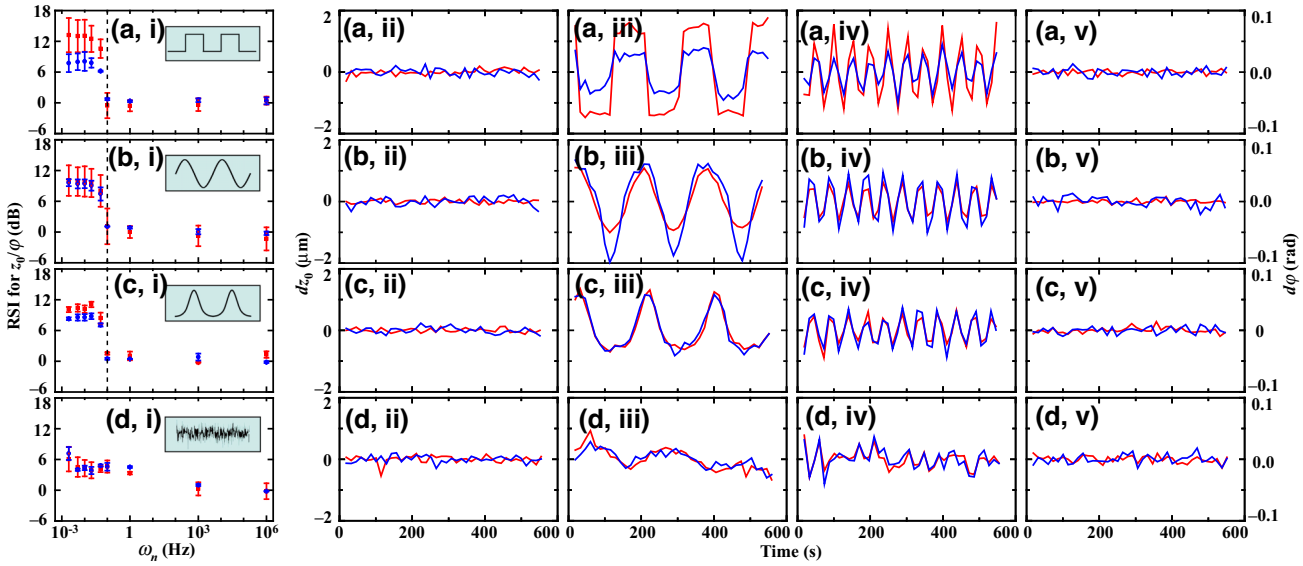

FIG. 2. The RSI detected by the phonon-laser sensor, where the injection-locking signal is input with frequency $\omega_i = 183.41$ kHz and amplitude $A_i = 7.5$ mV, the carrier signal is input with the same amplitude and frequency as the injection-locking signal, and the strength of the applied signal is $d_n = 0.5$. The different types of signals are listed in different rows with (a) the square-wave signal, (b) the sinusoidal-wave signal, (c) the Gaussian-wave signal, and (d) the bandwidth white-noise signal. The red and blue curves represent, respectively, the detection by the oscillation amplitude z_0 and phase φ of the phonon laser. Panels (i) demonstrate the RSI with respect to the modulation frequency ω_n, where the inset of each panel indicates the wave form of the signal employed in the corresponding experiment. The vertical dashed lines in (a)–(c) mark the frequency of 0.1 Hz. In each row, panels (ii)–(v) show the measured deviations of the oscillation amplitude $dz_0 = z_0 - \bar{z}_0$ and phase $d\varphi = \varphi - \bar{\varphi}$ with respect to (ii) the background noise and (iii)–(v) the artificially introduced signals, with (iii) $\omega_n = 5$ mHz, (iv) 50 mHz, and (v) 1 Hz. The error bars of the experimental data are the statistical standard deviation obtained from 40 measurements, each with a measurement time of 10 s.

(RSI) is given by

$$I = 10\log_{10}\frac{Y_n}{Y_0}, \tag{2}$$

where Y_n (Y_0) represents the mean deviation of the detected values in the presence (absence) of the additionally applied signals. As such, the error of the RSI can be calculated as follows:

$$\begin{aligned} dI &= \frac{\partial I}{\partial Y_n}dY_n + \frac{\partial I}{\partial Y_0}dY_0 \\ &= 10\left(\frac{dY_n}{Y_n \ln 10} - \frac{dY_0}{Y_0 \ln 10}\right) \\ &= \frac{10}{\ln 10}\left(\frac{dY_n}{Y_n} - \frac{dY_0}{Y_0}\right). \end{aligned} \tag{3}$$

B. Detection of electric field variations

Figure 2 demonstrates our detection of four types of artificially generated signals, including the square-wave signal, the sinusoidal-wave signal, the Gaussian-wave signal, and the white-noise signal. Experimentally, these signals are generated by the AWG and then applied by a capacitor on the AE electrode, the electrode to which the injection-locking signal applies. For a quantitative estimate, however, we first detect the background noise in the trap as a reference, corresponding to $d_n = 0$, prior to probing the additionally applied signals. Then we compare the measured amplitude or phase fluctuations of the phonon laser in the presence and absence of the artificially generated signals by employing the RSI. Experimentally, after the artificially generated signals are applied, we find that the phonon laser can detect the signals very sensitively when the signal frequency is less than 0.1 Hz, where the fluctuations of the phase and amplitude show the wave forms of the signals perfectly, particularly with more detailed characteristics for smaller values of ω_n. This is due to fact that in this case, the phonon laser only feels the signals with frequency less than Λ, as referred to above, and thus reconstructs the details of the signals. As such, this method of signal sensing provides the possibility of investigating the low-frequency signals, scrutinizing the shape of the signal in the time domain and hence functioning like an oscilloscope. Moreover, in contrast to other signals with RSI $= 0$ at $\omega_n = 0.1$ Hz, we observe RSI $= 6$ dB for the white-noise signal at that point. This is due to the fact that ω_n is the bandwidth of the white-noise signal and within the bandwidth, the white-noise signal involves all of the frequency components.

We further consider the situation with $\omega_n > 0.1$ Hz. In this case, we consider the signal with the sinusoidal

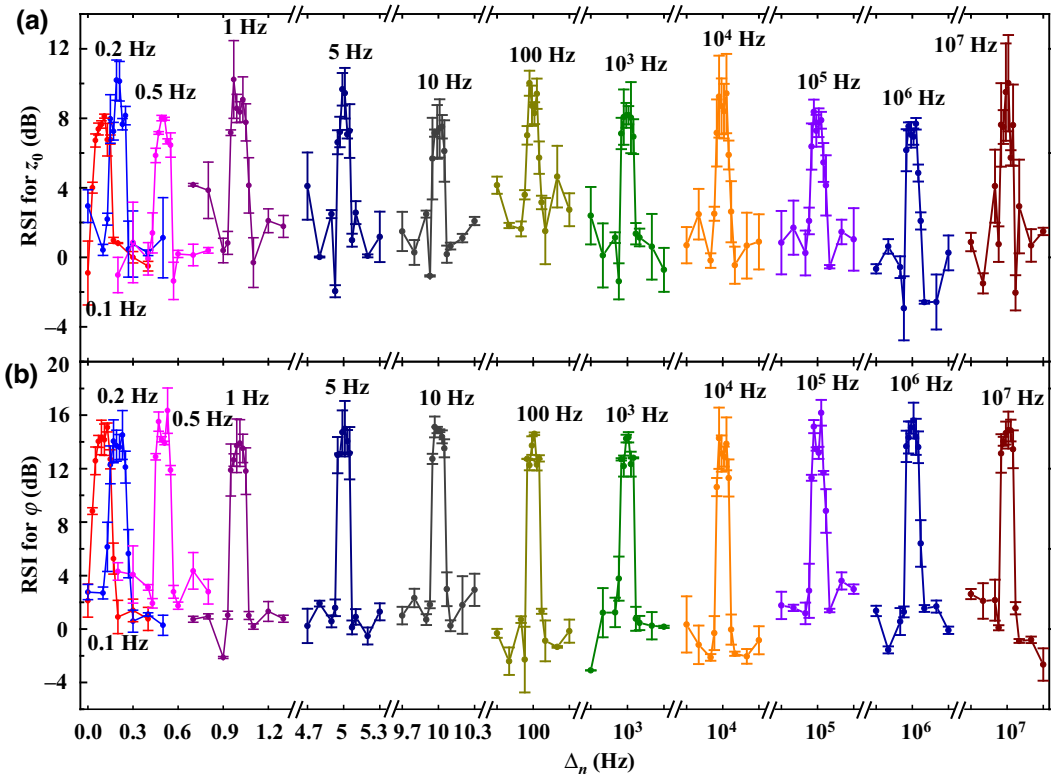

FIG. 3. The RSI of a sinusoidal-wave signal detected by the phonon-laser sensor, showing the fluctuations of (a) the oscillation amplitude and (b) the phase. The injection-locking signal is input with frequency $\omega_i = 183.41$ kHz and amplitude $A_i = 7.5$ mV. Compared with the injection-locking signal, the carrier signal is of the same amplitude but with the frequency shifted by Δ_n. The strength of the additionally applied signal is $d_n = 0.5$. The center frequencies of the additionally applied signal ω_n are labeled on the peaks of the curves detected (except for $\omega_n = 0.1$ Hz, which is labeled at the bottom for clarity) with a range of $\omega_n \pm 0.1$ Hz. The data points are experimental measurements, which are linked by solid lines to guide the eye. The error bars of the experimental data are the statistical standard deviation obtained from ten measurements, each with a measurement time of 10 s.

wave form as an example. Thus the modulated carrier signal can be decomposed into two frequency components, namely, $V_n(t) = d_n \sin\omega_n t \times A_i \sin(\omega_i + \Delta_n)t = d_n A_i[\sin(\omega_i + \Delta_n - \omega_n)t + \sin(\omega_i + \Delta_n + \omega_n)t]$. After the signal to be detected is input into the system, we scan the carrier signal by varying Δ_n and observe the variation of the oscillation amplitude and phase of the phonon laser. Experimentally, we vary the value of ω_n and then sweep Δ_n over the full frequency domain. Once the modulated signal enters the responding range (i.e., $|\omega_n - \Delta_n| < 0.1$ Hz), the phonon laser senses the signal, as presented in Fig. 3. Therefore, this method of signal detection functions like a frequency spectrograph and reproduces the shapes of the signals in the frequency domain.

C. Detection of white-noise signals

The white-noise signals produced artificially are close to the real noise in nature. To demonstrate that our detection is practical, in this subsection we focus on the detection of the white-noise signals.

To probe the various types of noise to the best effect, we have to optimize the working conditions of the phonon-laser sensor. To this end, we first test the best response of the sensor to the background noise in the trap by adjusting the characteristic parameters of the injection-locking signal. In Figs. 4(a) and 4(b), we observe that, with the increase of A_i, the mean deviation of z_0 first decreases and then increases but the mean deviation of φ just becomes smaller. By jointly evaluating the sensor performance from the error bars in both panels, we identify, with more trust on $\delta\varphi$, $A_i = 7.5$ mV to be optimal for our phonon-laser sensor. Based on this optimal value of A_i observed in Figs. 4(a) and 4(b), we further check the performance of the sensor by tuning the frequency ω_i of the injection locking. In Figs. 4(c) and 4(d), we find that the measured locking range is 400 Hz, which implies that our phonon laser could work when ω_i detuned from ω_z is smaller than ± 200 Hz. Moreover, we find that the optimal work point is at ω_z=ω_i, at which the error bars of the measurements are minimal.

With the optimal values of the characteristic parameters of the sensor as acquired in Figs. 4(a)–4(d), we take the white-noise signal with bandwidth of 50 mHz as an example to investigate the signal detection with the increase of

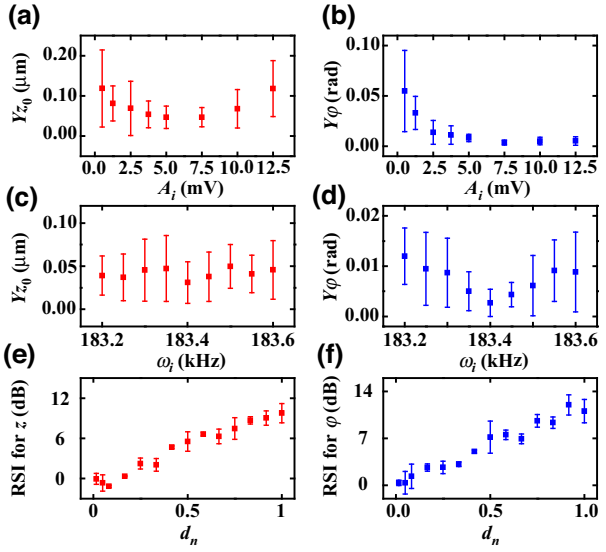

FIG. 4. (a)–(d) The detection of the white-noise signal with a bandwidth of 50 mHz by the phonon-laser sensor, with the objective of finding the optimal values of the characteristic parameters of the sensor. (a),(b) The mean deviations of the experimental data with respect to (a) the oscillation amplitude and (b) the oscillation phase of the phonon laser with respect to the amplitude of the injection-locking signal A_i. (c),(d) The same quantities as in (a) and (b) with respect to the frequency ω_i of the injection locking. (e),(f) The RSI relevant to the white-noise signal with respect to the signal strength d_n, detected from (e) the amplitude and (f) the phase of the phonon laser. The detections in (a) and (b), and then those in (c) and (d), lead to the optimal frequency $\omega_i = 183.41$ kHz and the optimal amplitude of the injection-locking signal, $A_i = 7.5$ mV, respectively. The detections in (e) and (f) are carried out using the optimal parameters found in (a)–(d). The error bars indicate the statistical standard deviation of the experimental data obtained from ten measurements, each with a measurement time of 10 s.

the signal amplitude in Figs. 4(e) and 4(f). Different from the other artificial signals with periodicity, the white-noise signal involves all of the frequency components. From the measurements of both the amplitude and phase, we see the rise of the RSI involving slight fluctuations. Moreover, from the observed values, we find that the lower bound of the detectable noise signal is $d_n = 0.083$. The observations in both Fig. 4(e) and Fig. 4(f) are similar and linear, indicating the feasibility and credibility of using the ion phonon laser as a single-atom sensor to detect the electric field fluctuations. Further scrutiny of the fluctuations might be useful in order to understand the electric field fluctuations in more detail.

Based on the results acquired from Fig. 4, we further check the characteristics of the white-noise signal when our sensor is under the best detection conditions. In contrast to the frequency spectrograph for the periodically varying signals in Fig. 3, here we examine the detecting ability of the sensor for an aperiodic noise signal. Using

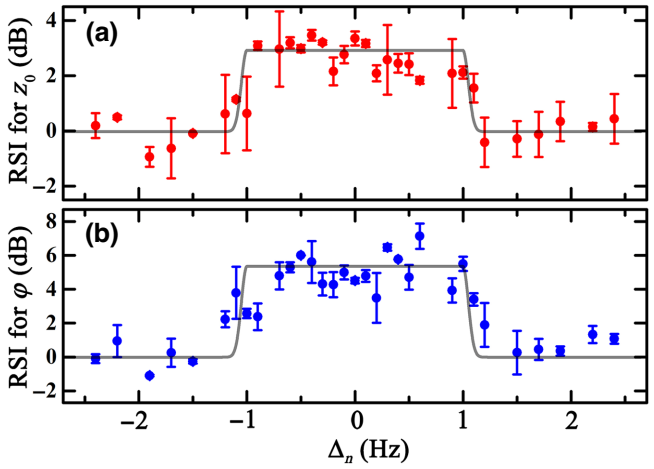

FIG. 5. The RSI of the white-noise signal detected by the phonon-laser sensor with respect to the (a) oscillation amplitude and (b) the phase with respect to Δ_n. The injection locking is with frequency $\omega_i = 183.41$ kHz and amplitude $A_i = 7.5$ mV and the white-noise signal is with $d_n = 0.5$ and bandwidth $= 1$ Hz. The gray lines are the fitting of the experimental data to guide the eye. The error bars indicate the statistical standard deviation of the experimental data obtained from ten measurements, each with a measurement time of 10 s.

the measured values of the mean deviations with respect to z_0 and φ, we demonstrate in Fig. 5 the detection of the white-noise signal with a bandwidth of 1 Hz by sweeping Δ_n, the envelope of which is spread by ± 1 Hz with respect to $\Delta_n = 0$. The experimental values, i.e., the dots, reflect the fluctuations of different frequency components within the bandwidth. Since the white-noise signal is very close to the real noise, these observations confirm the practicability of our sensor, which would work for the detection of very complicated signals.

IV. DISCUSSION

Above, we are sensing artificially generated signals, which are attached to the carrier signals in our measurements and are different from any independent signal that exists in nature. Even the white-noise signals, although very close to real noise, are actually different from real environmental noise. To probe an independent signal, the frequency of the signal is required to be close to that of the injection signal, satisfying $|\omega_n - \omega_i| < \Lambda$. In practice, if the signals to be detected could be efficiently collected and applied on the carrier signals, our sensor would definitely probe them by shifting the frequency of the carrier signal, following the same steps as in Fig. 3.

Moreover, we also detect the background noise in the trap, which is real environmental noise with components of frequencies close to ω_i. Following this idea, if we hope to detect real environmental noise, we may tune both ω_z and ω_i over a wide range of frequencies. However, what we quantify for the background noise is the RSI, i.e., the

deviation of the oscillation amplitude or phase, which can be employed as a prior calibration for detecting the injected signals but is not the conventional approach for noise detection. To follow the conventional route, e.g., using the power spectral density to characterize the various types of noise, we might have to measure the minimum force due to the electric field variation, as in Ref. [17]. In our case here, the sensitivity of detecting such a force by the phonon-laser technique is about 64 yN/$\sqrt{\text{Hz}}$, implying the achievement of a noise spectral density of 1.6×10^{-7} V^2/m^2 Hz [24]. We note recent efforts to explore the detection of the noise spectra of electric fields using harmonic oscillators [25–27]. The basic ideas in these works are enacted on harmonic oscillators with the preparation of cold initial states and variation of the resonance frequencies, which are directly relevant to laser-cooled ions confined in electromagnetic fields. Therefore, the accuracy of these methods is mainly limited by the temperature of the ions, e.g., sideband cooling of the trapped ions is the prerequisite of the techniques demonstrated [26,27].

In this context, since our sensing technique works without the prerequisite of sideband cooling, we may consider our technique to be more practical for some tasks, e.g., as an everyday check of the background noise in the trapped-ion system. We may take the optimal value of the noise sensing as Y_0 in Eq. (A2) and thus the RSI reflects the working conditions of the trapped-ion system on a certain day with the noise-sensing value of Y_n. To this end, we need to constantly improve this technique. Hopefully, our detection method will be able to be implemented more quickly after the technique is further optimized, e.g., with a higher fluorescence collection efficiency and better stability conditions. Enhancement of the fluorescence collection efficiency is experimentally feasible if the trapping system is more compact, with a larger solid angle for the collection of spontaneously scattering photons [28]. The stability conditions could be improved by suppressing the secular frequency drift resulting from the electrode voltage drift [29] and cleaning the electrode surfaces [30]. With this optimization, we anticipate that the detection time for each data point would be less than 0.1 s and, meanwhile, higher-quality detection for the electric field fluctuation would be possible. Thus the sensitivity of the ac electric force would hopefully reach 10 yN/$\sqrt{\text{Hz}}$ or even less, implying the achievement of a noise spectral density of, or lower than, the order of magnitude of 10^{-9} V^2/m^2 Hz.

V. CONCLUSIONS

In summary, we demonstrate a practical technique for the detection of alternating electric signals using a single-atom sensor. Since it works with no need of sideband cooling and is based on very sensitive optical detection, the technique is very practical and is readily implementable in trapped-ion systems to present the fluctuations of input electric signals in the time and space domains. Also, it may be possible to utilize the technique for the detection of real environmental noise, e.g., as a routine means for diagnosing background noise in ion-trap systems. Moreover, this technique can be extended to other ions, particularly favoring lighter ions due to their greater sensitivity to ac field forces [17], and even applied to other systems involving the phonon laser, such as the optical-tweezer system [31].

ACKNOWLEDGMENTS

This work was supported by the Special Project for Research and Development in Key Areas of Guangdong Province under Grant No. 2020B0303300001 and by the National Natural Science Foundation of China under Grants No. U21A20434, No. 12074346, No. 12074390, No. 11835011, No. 11804375, and No. 11804308.

APPENDIX A: ACQUISITION OF z_0 AND φ

We briefly introduce our approach to rapidly acquiring the value of z_0 by fitting the recorded photons scattered from the ion [17]. We assume that the phase φ and the amplitude z_0 of the oscillator are constants during our measurement. Under irradiation by the 397-nm laser beams, the scattering rate ρ_j at time t is given by [10]

$$\rho_j(t) = \frac{\Gamma s_j/(4\pi)}{1 + s_j + 4\left[\frac{\Delta_j - k_j\,\omega_i z_0\cos(\omega_i t+\varphi)}{\Gamma}\right]^2}, \tag{A1}$$

where Γ is the decay rate of $P_{1/2}$, k_j is the wave vector, Δ_j denotes the detuning, and s_j represents the saturation parameter. Due to the two 397-nm laser beams with different detunings in our experiment, the total scattering rate is $\rho(t) = \rho_1(t) + \rho_2(t)$. Since the experimental data include the influence of different types of noise in the experimental system, we employ the Gaussian term $G(t)$ to fit the curve of $P(t)$ with a convolution function,

$$P(t) = \alpha\rho(t) * G(t) + \beta, \tag{A2}$$

where $G(t) = (1/\sqrt{2\pi}\sigma_t)\exp[-t^2/(2\sigma_t^2)]$, in which σ_t is the degree of time dispersion. α and β represent the factors with respect to the measurement time, the fluorescence collection efficiency η, the background photons, and the number of unit time intervals n, as well as the signal-to-noise ratio relevant to the background light. These parameters can be determined experimentally prior to acquiring the oscillation amplitude z_0 and phase φ [17].

APPENDIX B: RESPONDING RANGE OF THE PHONON-LASER SENSOR

In order to detect the responding range Λ of the phonon-laser sensor, we introduce an alternating signal

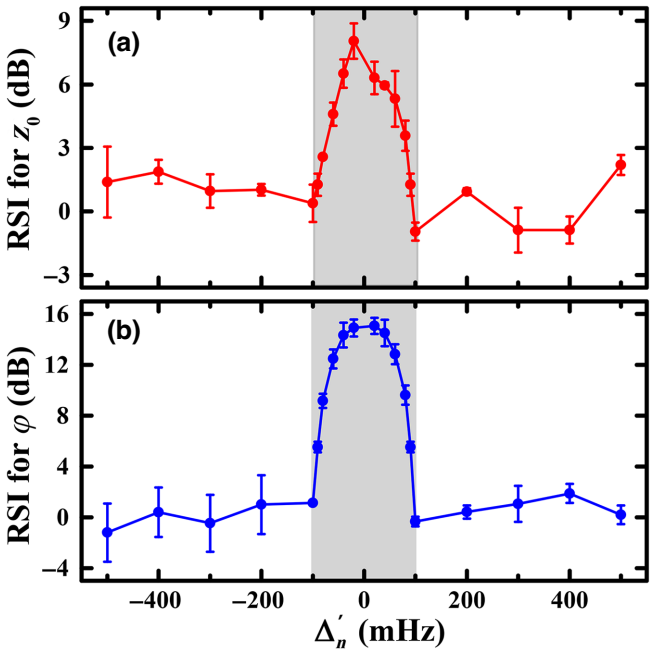

FIG. 6. The detection of the responding range Λ of the phonon-laser sensor using (a) the oscillation amplitude and (b) the phase, where $\Delta_n' = \omega_n - \omega_i$. The data points are linked with the solid lines to guide the eye. Other parameters: $A_i = 7.5$ mV and $A_n = 1.9$ mV.

with the sinusoidal form of $A_n \sin \omega_n t$ to the electrode AE. By sweeping the signal frequency ω_n with respect to the injection-locking signal frequency ω_i, we find from both the oscillation amplitude and phase, as shown in Fig. 6, a spread of ± 0.1 Hz with respect to $\Delta_n' = 0$, indicating that the responding range Λ of the phonon laser is 0.1 Hz.

Since our measurement of each data point takes a time of 10 s, it seems that Λ is simply the inverse of this measurement time. Further investigation of Λ to elucidate the physics involved is to be expected.

[1] C. Gardiner and P. Zoller*Quantum Noise* (Springer, New York, 2004).

[2] E. L. Hahn, Spin echoes, Phys. Rev. **80**, 580 (1950).

[3] H. Y. Carr and E. M. Purcell, Effects of diffusion on free precession in nuclear magnetic resonance experiments, Phys. Rev. **94**, 630 (1954).

[4] L. Viola, E. Knill, and S. Lloyd, Dynamical Decoupling of Open Quantum Systems, Phys. Rev. Lett. **82**, 2417 (1999).

[5] G. S. Uhrig, Keeping a Quantum Bit Alive by Optimized π-Pulse Sequences, Phys. Rev. Lett. **98**, 100504 (2007).

[6] M. J. Biercuk, H. Uys, A. P. Vandevender, N. Shiga, W. M. Itano, and J. J. Bollinger, Optimized dynamical decoupling in a model quantum memory, Nature (London) **458**, 996 (2009).

[7] M. Brownnutt, M. Kumph, P. Rabl, and R. Blatt, Ion-trap measurements of electric-field noise near surfaces, Rev. Mod. Phys. **87**, 1419 (2015).

[8] C. L. Degen, F. Reinhard, and P. Cappellaro, Quantum sensing, Rev. Mod. Phys. **89**, 035002 (2017).

[9] N. P. de Leon, K. M. Itoh, D. Kim, K. K. Mehta, T. E. Northup, H. Paik, B. S. Palmer, N. Samarth, S. Sangtawesin, and D. W. Steuerman, Materials challenges and opportunities for quantum computing hardware, Science **372**, 6539 (2021).

[10] D. Leibfried, R. Blatt, C. Monroe, and D. Wineland, Quantum dynamics of single trapped ions, Rev. Mod. Phys. **75**, 281 (2003).

[11] K. Vahala, M. Herrmann, S. Knünz, V. Batteiger, G. Saathoff, T. W. Hänsch, and T. Udem, A phonon laser, Nat. Phys. **5**, 682 (2009).

[12] I. S. Grudinin, H. Lee, O. Painter, and K. J. Vahala, Phonon Laser Action in a Tunable Two-Level System, Phys. Rev. Lett. **104**, 083901 (2010).

[13] M. Ip, A. Ransford, A. M. Jayich, X. Long, C. Roman, and W. C. Campbell, Phonon Lasing from Optical Frequency Comb Illumination of Trapped Ions, Phys. Rev. Lett. **121**, 043201 (2018).

[14] B. He, L. Yang, and M. Xiao, Dynamical phonon laser in coupled active-passive microresonators, Phys. Rev. A **94**, 031802 (2016).

[15] M. R. Hush, W. Li, S. Genway, I. Lesanovsky, and A. D. Armour, Spin correlations as a probe of quantum synchronization in trapped-ion phonon lasers, Phys. Rev. A **91**, 061401 (2015).

[16] F. Dominguez, I. Arrazola, J. Doménech, J. S. Pedernales, L. Lamata, E. Solano, and D. Rodriguez1, A single-ion reservoir as a high-sensitive sensor of electric signals, Sci. Rep. **7**, 8336 (2017).

[17] Z.-C. Liu, Y.-Q. Wei, L. Chen, J. Li, S.-Q. Dai, F. Zhou, and M. Feng, Phonon-Laser Ultrasensitive Force Sensor, Phys. Rev. Appl. **16**, 044007 (2021).

[18] M. G. House, Analytic model for electrostatic fields in surface-electrode ion traps, Phys. Rev. A **78**, 033402 (2008).

[19] W. Wan, H. Y. Wu, L. Chen, F. Zhou, S. J. Gong, and M. Feng, Demonstration of motion transduction in a single-ion nonlinear mechanical oscillator, Phys. Rev. A **89**, 063401 (2013).

[20] Z.-C. Liu, L. Chen, J. Li, H. Zhang, C. Li, F. Zhou, S.-L. Su, L.-L. Yan, and M. Feng, Structural phase transition of the ion crystals embedded in an optical lattice, Phys. Rev. A **102**, 033116 (2020).

[21] L. L. Yan, S. L. Su, and M. Feng, Analytical investigation of one-dimensional Doppler cooling of trapped ions with Λ-type configuration, Phys. Rev. A **100**, 033418 (2019).

[22] S. Knünz, M. Herrmann, V. Batteiger, G. Saathoff, T. W. Hänsch, K. Vahala, and T. Udem, Injection-Lock of a Trapped-Ion Phonon Laser, Phys. Rev. Lett. **105**, 013004 (2010).

[23] The statement in this paragraph is true for the additionally applied signals with various forms of periodic functions but not for the white-noise signal, in which ω_n is the bandwidth of the white noise.

[24] With respect to the work published in Ref. [17], we are further optimizing this sensing technique with the phonon laser to achieve more sensitive detection of the ac electric force. The paper is in preparation.

[25] D. Goldwater, P. F. Barker, A. Bassi, and S. Donadi, Quantum Spectrometry for Arbitrary Noise, Phys. Rev. Lett. **123**, 230801 (2019).

[26] A. R. Milne, C. Hempel, L. Li, C. L. Edmunds, H. J. Slatyer, H. Ball, M. R. Hush, and M. J. Biercuk, Quantum Oscillator Noise Spectroscopy via Displaced Cat States, Phys. Rev. Lett. **126**, 250506 (2021).

[27] J. Keller, P.-Y. Hou, K. C. McCormick, D. C. Cole, S. D. Erickson, J. J. Wu, A. C. Wilson, and D. Leibfried, Quantum Harmonic Oscillator Spectrum Analyzers, Phys. Rev. Lett. **126**, 250507 (2021).

[28] R. Maiwald, D. Leibfried, J. Britton, J. C. Bergquist, G. Leuchs, and D. J. Wineland, Stylus ion trap for enhanced access and sensing, Nat. Phys. **5**, 551 (2009).

[29] K. G. Johnson, J. D. Wong-Campos, A. Restelli, K. A. Landsman, B. Neyenhuis, J. Mizrahi, and C. Monroe, Active stabilization of ion trap radiofrequency potentials, Rev. Sci. Instum. **87**, 053110 (2016).

[30] D. T. C. Allcock, L. Guidoni, T. P. Harty, C. J. Ballance, M. G. Blain, A. M. Steane, and D. M. Lucas, Reduction of heating rate in a microfabricated ion trap by pulsed-laser cleaning, New J. Phys. **13**, 123023 (2011).

[31] R. M. Pettit, W. Ge, P. Kumar, D. R. Luntz-Martin, J. T. Schultz, L. P. Neukirch, M. Bhattacharya, and A. N. Vamivakas, An optical tweezer phonon laser, Nat. Photonics **13**, 402 (2019).